# Insight into Stable, Concentrated Radicals: from Sulfur-functionalized Alkyne-rich Crystalline Frameworks to Simple Alkyne Motifs

*Dong-Ling Kuang, Jian-Rong Li, Jieying Hu, Lai-Hon Chung, Parijat Borah, Zhengtao Xu* and Jun He**

School of Chemical Engineering and Light Industry, Guangdong University of Technology, Guangzhou 510006, Guangdong, China.

Institute of Materials Research and Engineering (IMRE), Agency for Science, Technology and Research (A*STAR), 2 Fusionopolis Way, Singapore, 138634, Republic of Singapore.

Keywords: porous solids, coordination polymers, free radicals, nanographene, domino benzannulation

Abstract: Organic radicals feature versatile unpaired electrons key for photoelectronic and biomedical applications, but remain difficult to access in stable concentrated forms. We disclose easy generation of stable, concentrated radicals from various alkynyl phenyl motifs, including 1) sulfur-functionalized alkyne-rich organic linkers in crystalline frameworks; 2) the powders of these molecules alone; 3) simple diethynylbenzenes. For Zr-based framework, generation of radical-rich crystalline framework was achieved by thermal annealing in the range of 300–450 °C.

For terminal alkynes, electron paramagnetic resonance signals (EPR; indicative of free radicals) arise after air exposure or mild heating (*e.g.*, 70 °C). Further heating (*e.g.*, 150 °C for 3 hours) raises the radical concentrations up to 3.30 mol $kg^{-1}$. For the more stable internal alkynes, transformations into porous radical solids can also be triggered, albeit at higher temperatures (*e.g.*, 250 to 500 °C). The resulted radical-containing solids are porous, stable to air as well as heat (up to 300–500 °C) and exhibit photothermal conversion capacity. The formation of radicals can be ascribed to extensive alkyne cyclizations, forming defects, dangling bonds and the associated radicals stabilized by the polycyclic π-systems.

## 1. INTRODUCTION

Persistent stable organic free radicals are prized in chemistry and have since long been actively pursued.[1-2] Such efforts are driven not only by the curious open-shell structure of radicals (*e.g.*, as compared to the common octet), but also by broad applications covering polymer functionalization,[3-9] solar cells,[10-11] magnetic materials design,[12-15] and bioimaging/cancer therapy.[16-17] But the stabilization of organic radicals remains difficult—after all, it is the chemist's instinct to draw bonds between unpaired electrons! Metal-organic frameworks (MOFs), constructed by metal nodes and organic linkers, represent a group of rising stars holding well-defined structures, rich functionalities and tunable porosity;[18-22] hence these are ideal platforms for formation and stabilization of radicals.[23-24] In practice, elaborate molecular design and syntheses are often entailed, including steric protection[2, 25-26] and large delocalization of the unpaired electron,[27-32] as well as specialized functionality as in the recently developed stable radical systems (*e.g.*, derived from 1,4-dithiin building blocks).[33-34]

Amidst the intense works on radicals, the common charcoal and carbon black have been largely missing in the picture. These are known to contain radical species (albeit in vanishing concentrations; below 1 ppm), and have, for example, been explored for in vivo electron paramagnetic resonance (EPR) oxygen sensing (oximetry) by the Gallez group.[35-36] For broader applications, however, higher concentrations of radical centers would be helpful. On the one hand, the low concentration of radicals in carbon black is expected, because of the high carbonization temperatures (> 800 °C) in which the reactive radical species can barely survive; we therefore hypothesize lower temperatures to be a key to more concentrated radicals. On the other hand, it may be necessary to design reactive carbon-rich precursors that can carbonize or graphitize (*e.g.*, *via* domino cyclization reactions) at lower temperatures, so as to afford the carbon/graphene scaffold that shelters the unpaired electrons (*e.g.*, by way of defect/trap sites or delocalization).

This hypothesis connects naturally to our ongoing works on alkyne annulation.[37-42] In solution chemistry, similar cyclizations (*e.g.*, Bergman cyclization for 1,2-dialkynylarenes) are intended for well-defined, discrete molecular products, and metal catalysts/hydrogen donors are used for promoting selectivity and minimizing side reactions (*e.g.*, from the reactive radical intermediates).[43-48] Our motivation, however, lies in the solid state; notice that in the solid state, cascade cyclizations to form polycyclic aromatics have been conducted, but, curiously, with no mention of radical species in the annulated products.[48-50] Specifically, we build the alkyne units into the linker molecules of coordination (or covalent) frameworks: by cyclizing the alkyne-rich bridging ligands, we aim to generate nanographene motifs as large-π functions (for electronic properties) and covalent bridges (for stabilizing the coordination net). As we are detached from targeting a specific molecular product, we simply apply heat to the coordination solid--without using metal catalysts or hydrogen donors; notably also, we do not normally heat to the fully

carbonizing temperatures of above 800 °C, but instead range lower at 250–500 °C. Such mild but broad heating profiles preserve the crystalline order of the coordination scaffold on the one hand and offer control over the degree of graphitization on the other. The domino cyclizations among the dense alkyne arrays are extensive, and the resultant nanographene components are often disordered. While working towards better-defined graphitization (*e.g.*, to emulate the coveted 3D graphenes of Schwarzites), we have discovered that the products of *ortho*-dialkynyl thermocyclization often feature strong EPR signals indicative of concentrated organic radicals. We have followed this lead and found, to our surprise, that even simple dialkynyl molecules, upon standing in air, can form organic radicals stable to heat, air, and water.

## 2. EXPERIMENTAL SECTION

The general procedure and synthetic procedures of linker ($H_2$**L3**) and alkyne molecules (**M1**, **M2** and **M3**) as well as their thermal treatment are included in the Supporting Information.

*Crystallization of Zr**L3**:* Ligand $H_2$**L3** (3 mg) and a DEF (0.2 mL) solution of $ZrOCl_2$•$8H_2O$ (1.8 mg, 2 *eq*.) and trifluoroacetic acid (12.5 μL, about 20 molar equivalents to $ZrOCl_2$•$8H_2O$) were added in a Pyrex glass tube (soda lime, 8 mm OD, 6 mm ID). The tube was flame-sealed and heated at 130 °C in an oven for 48 hours and cooled to room temperature to afford orange octahedron-shaped crystals. The crystals were washed with DMF (3 × 2 mL) and $CH_3CN$ (3 × 2 mL), then evacuated at room temperature for 2 hours to obtain the as-made sample of Zr**L3** (donated as Zr**L3**-as) (3.2 mg, 73.6% yield based on $H_2$**L3**). Elemental analysis found C (49.90%), H (3.50%), N (1.47%), O (15.05%) and S (16.62%) for as-made Zr**L3**, this analysis fits the formula to be $Zr_6O_4(OH)_8(H_2O)_4$(**L3**)$_{3.3}(CF_3COO)_{1.4}(C_3N_7NO)_{5.5}(H_2O)_{11}$ (Mw 5067.40), calculated: [C (49.94%), H (4.15%), N (1.52%), O (15.31%) and S (16.70%) and Zr (10.80%)].

*Activation of Zr**L3**:* The crystals were soaked in $CH_3CN$ (3 × 3 mL, replaced by fresh $CH_3CN$ every 12 hours) at 70 °C for solvent exchange. The resulting crystals were filtered and then evacuated at 85 °C for 12 hours to obtain the activated sample of Zr**L3** (donated as Zr**L3**-ac). Elemental analysis found C (52.178%), H (3.316%) and N (0.215%) for activated Zr**L3**, this analysis fits the formula to be $Zr_6O_4(OH)_8(H_2O)_4(\mathbf{L3})_{3.3}(CF_3COO)_{1.4}$ (Mw 4467.21), calculated: [C (52.21%), H (3.34%) and Zr (12.25%)].

*Thermocyclization of Zr**L3**:* Zr**L3** was heated in Quartz tube furnace in $N_2$ atmosphere for 2 hours at 300, 350, 400 and 450 °C, respectively. Heating rate: 5 °C/min. The resultant powder was denoted as Zr**L3**-T (T = 300, 350, 400 or 450).

*Photothermal Conversion Measurement:* Photothermal measurements of Zr**L3** and Zr**L3**-T (T = 300, 350, 400 or 450 °C) samples (30 mg) were performed by using the xenon lamp (AM 1.5 G, PLS-SXE300+). The temperature response of the samples was measured with an IR thermal camera (MAG14, Shanghai Magnity Technologies Co. Ltd., China).

## 3. RESULTS AND DISCUSSION

The initial suspicion about possible radical presence was raised by the sulfur-rich molecule $H_2$**L3** (Figure 1). The design of $H_2$**L3** followed the previous design of backfolded alkyne side arms, *e.g.*, for growing crystalline MOF structures and subsequently thermocyclizing the alkyne groups to generate nanographene functions.[38-42] The numerous sulfur(methylthio) groups, on the other hand, were originally meant for functionalization such as facilitating metal uptake and oxidation treatment. As sulfur atoms are associated with many functional radical species in discrete molecules as well as in extended structures,[51-54] we had wondered if the thermocyclizing the sulfur-rich MOF solid of Zr**L3** led to radical species.

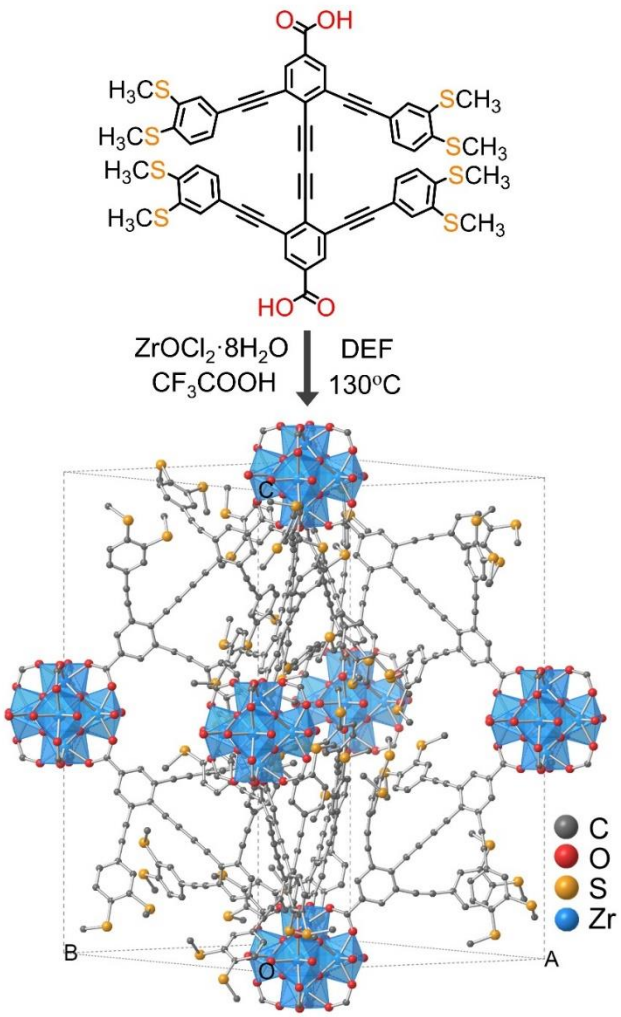


**Figure 1.** Schematic showing the structure of ligand $H_2$**L3**, and solvothermal synthesis of Zr**L3** network featuring **bcu** topology (shown as an octahedral cage based on Zr–O clusters and **L3** linkers).

Zr**L3** was grown solvothermally in DEF (*N,N*-diethylformamide) using $H_2$**L3**, $ZrOCl_2 \cdot 8H_2O$ and $CF_3COOH$ as organic linker, metal source and modulator, respectively (Figure 1). Powder X-ray diffraction (PXRD) pattern of as-made Zr**L3** reveals a tetragonal unit cell ($a$ = 24.284, $c$ = 33.770 Å; Figure 2a; details of refinement included in the Supporting Information), isomorphic with previously reported Zr**L1** bearing the peaks at 4.40, 5.10, 7.34, 8.62, and 9.01° indexed as (101), (110), (112), (211), and (202), respectively.[42] The framework structure features 8-connected

$Zr_6O_4(OH)_8(H_2O)_4$ clusters bridged by linker **L3** and adopts a **bcu** topology, with the octahedral cage missing four equatorial edges to provide structural flexibility (see PXRD patterns in Figure S3) and give rise to a tetragonal lattice.

Fourier transform infrared (FT-IR) spectra show that the C=O stretch of $H_2$**L3** at 1695 $cm^{-1}$ shifts to 1599 $cm^{-1}$ after coordinating the Zr–O cluster (Figure S4). $^1H$ NMR spectrum obtained from digestion of Zr**L3** in NaF/DCl/DMSO-$d_6$ consistent with that of pure $H_2$**L3**, revealing that linker **L3** did not decompose during the solvothermal synthesis (Figure S5). Elemental analysis (EA) data can be fitted by the formula of $Zr_6O_4(OH)_8(H_2O)_4$(**L3**)$_{3.3}(CF_3COO)_{1.4}$ for Zr**L3**, which is further supported by thermogravimetric analysis (TGA, Figure S6). The linker deficiency (1.4/8 = 17.5%) of Zr**L3** is likely due to the steric hindrance from the long and rigid alkyne side arms on the **L3** linker.

Thermal treatments of the light-yellow Zr**L3** solid at 300, 350, 400 and 450 °C formed the black solids of Zr**L3**-300, Zr**L3**-350, Zr**L3**-400 and Zr**L3**-450, respectively (see Figure S7 for photographs). As shown in the UV–Vis–NIR absorption spectra (Figure 2b), absorption of Zr**L3** exhibits more significant red shift along with thermal treatment at higher temperatures and even reaches near-IR (NIR) region (*e.g.*, absorption edges beyond 1800 nm for Zr**L3**-400 and Zr**L3**-450). While Zr**L3** feature distinct IR peak at 2202 $cm^{-1}$ for the alkyne units, such alkyne signal is absent in samples of Zr**L3**-300, Zr**L3**-350, Zr**L3**-400, Zr**L3**-450, consistent with the cyclization reaction of the closely positioned alkyne groups (Figure 2c). Further evidence of aromatization comes from solid state $^{13}C$ NMR (Figure 2d). The two broad signals at 129.83 and 136.13 ppm are attributed to aromatic C atoms and the crosslinking C–S carbons. The massive cyclization here is, however, complex and multifarious, and therefore difficult to characterize; to illustrate the various plausible cyclization steps, we attach a tentative scheme in Figure S8. The weak signal at 172.17

ppm belongs to the two carboxyl carbons of linker, while the peaks at 14.88 ppm are consistent with retained –$SCH_3$ carbons. All four heated samples are crystalline (Figure 2a) and remain porous, with increased $CO_2$ adsorption capacity and Langmuir surface area from 104.11 $m^2/g$ for activated Zr**L3** to 448.71 $m^2/g$ for Zr**L3**-450 (Figure 2e).

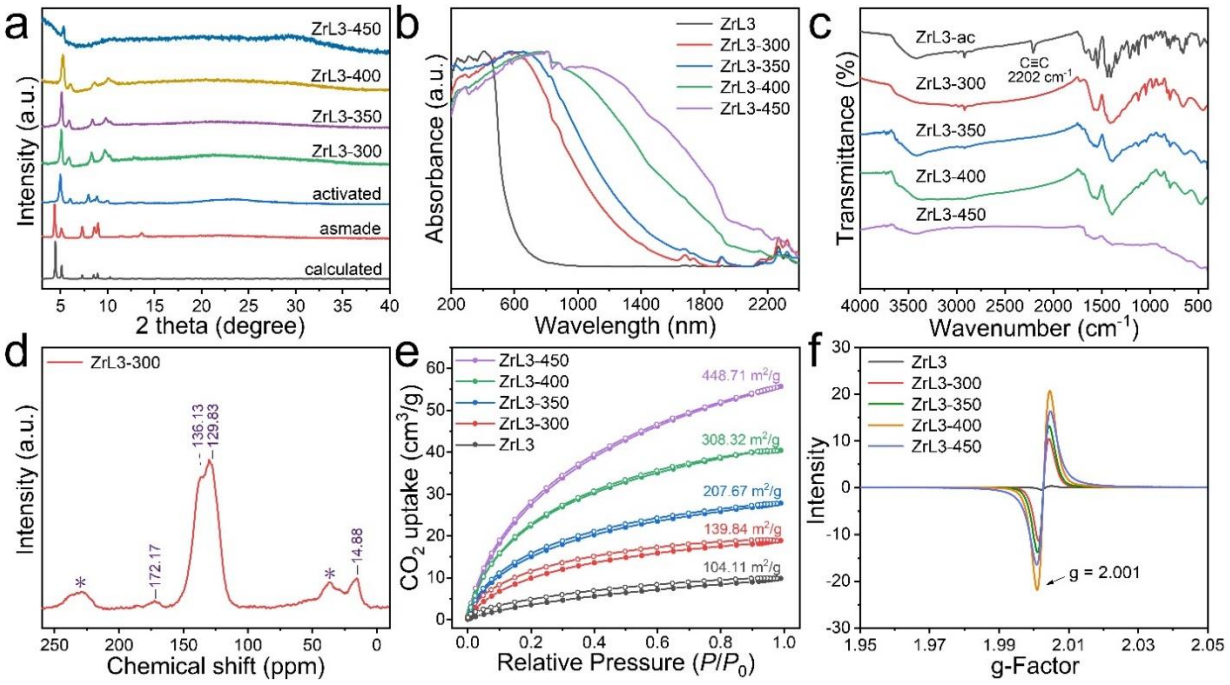


**Figure 2.** (a) PXRD patterns, (b) UV-vis-NIR absorption spectra and (c) FT-IR spectra of Zr**L3** before and after thermocyclization. (d) Solid-state $^{13}C$ NMR spectrum of Zr**L3**-300 (the asterisks indicate spinning side bands). (e) $CO_2$ adsorption and desorption isotherms at 273 K and (f) solid-state EPR spectra at room temperature for activated samples of Zr**L3**, Zr**L3**-300, Zr**L3**-350, Zr**L3**-400 and Zr**L3**-450.

The key evidence of organic radical species comes from the strong EPR signals of the heated samples, Zr**L3**-300, Zr**L3**-350, Zr**L3**-400 and Zr**L3**-450, as compared with the weak EPR of the as-made Zr**L3** solid (Figure 2f). From Zr**L3**-300, Zr**L3**-350 to Zr**L3**-400, the signal steadily increases, indicating the correspondingly greater concentration of radicals as a function of the

temperature; at higher temperatures, however, the EPR signal becomes weaker, as is shown in Zr**L3**-450, which can be ascribed to higher temperature driving the formation of products closer to the thermodynamic, stable, radical-free state. The radicals of these samples are stable in air and acids. For example, treatment with HF (this etches away the $Zr^{4+}$ ions) destroys the crystalline order as shown by PXRD, but the EPR signal persists (Figure S9).

In addition to the EPR measurements, variable-temperature magnetic susceptibility studies of Zr**L3** and Zr**L3**-400 were conducted at a dc field of 1000 Oe at 2–300 K to further characterize these radical-containing solids. As illustrated by $\chi_M T$ *versus* T plots (Figure S10), the $\chi_M T$ of Zr**L3** is 0.39 $cm^3$ K $mol^{-1}$ at 300 K and decreases to 0.005 $cm^3$ K $mol^{-1}$ at 2 K. As for Zr**L3**-400 [molar mass = 3911.94: 87.57% of Zr**L3**, based on TG curve in Figure S6), the $\chi_M T$ is 17.24 $cm^3$ K $mol^{-1}$ at 300 K and decreases to 0.13 $cm^3$ K $mol^{-1}$ at 2 K. This $\chi_M T$ value of 16.85 $cm^3$ K $mol^{-1}$ can be ascribed to the organic radicals in Zr**L3**-400. The corresponding effective magnetic moment, $\mu_{eff} = 8\chi_M T^{1/2}$ = 11.61 B.M., closely matches ten unpaired electrons: $\mu_{eff} = g[S(S + 1)]^{1/2}$ = 10.95 (S = 10/2 = 5, with $g$ = 2). As Zr**L3** and Zr**L3**-400 each contain 3.3 linkers in the asymmetric unit, each linker bears roughly 3 unpaired electrons. With this information, the radical concentration of Zr**L3**-400 was calculated to be 2.56 mol/kg (obtained by: 1/3.91194 kg $mol^{-1}$ × 10). With the radical concentration in Zr**L3**-400 thus quantified, it can be quantitatively correlated with the measured EPR intensity. This relationship is employed to calculate (from the EPR intensities) the radical concentrations of other samples in this study (Table S1).

The radical can also form without using the elaborate, ordered Zr**L3** structure--namely, simply by heating the sodium salt $Na_2$**L3** (Scheme S2, prepared from simple mixing of $H_2$**L3** and NaOH) and even the solid sample of the $H_2$**L3** molecule. Like the Zr**L3** solid, both $Na_2$**L3** and $H_2$**L3** exhibit similar blackening and disappearing of the alkyne groups (*e.g.*, as per IR, Figure S11) upon heating

(*e.g.*, 300 °C or above). After heating at between 400 and 500 °C, the EPR signal of $Na_2$**L3** (*e.g.*, $Na_2$**L3**-400 and $Na_2$**L3**-500) appear to be stronger than those of Zr**L3** (Figure 3a), even though at higher temperatures (*e.g.*, 600 °C), the radical is also significantly suppressed for $Na_2$**L3**. The EPR signals of the $H_2$**L3** samples appear to be similar in strength to those of Zr**L3** (Figure 3b). It remains to be elucidated why $Na_2$**L3** exhibits stronger EPR signals.

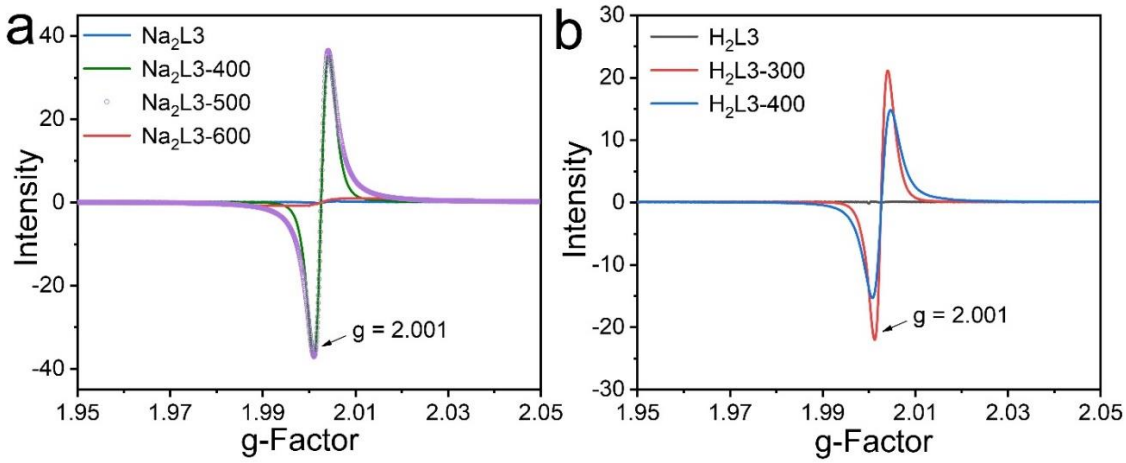


**Figure 3.** Solid-state electron paramagnetic resonance (EPR) spectra at room temperature of (a) $Na_2$**L3**, $Na_2$**L3**-400, $Na_2$**L3**-500 and $Na_2$**L3**-600, and (b) $H_2$**L3**, $H_2$**L3**-300 and $H_2$**L3**-400.

We then took a leap of faith, and tested the simple alkyne molecules of **M1** (tetraethynylbenzene), **M2** (diethynylbenzoic acid), and **M3** (1,4-diethynylbenzene). Because of the high proportion of the alkyne units in these molecules, safety measures against explosion are needed, especially for freshly prepared samples. For example, the powder of fresh **M1** explodes when heated to 100 °C (in air or $N_2$); but air exposure tempers its tendency to explode: an exposure of 5 hours (spread out on a Petri dish) is sufficient to obviate explosion in subsequent heat treatment. Alternatively, one can heat the sample at 70 °C for a few hours (*e.g.*, 3 hours; in $N_2$), then proceed to higher temperature; this also eliminates explosion.

As it were, the powder of **M1** is not stable in air: at room temperature, it turns from light yellow to brown over a few hours, with its EPR spectrum already showing signal for radical species (Figure 4d, exposure time 72 hours). The EPR signal strengthens significantly after mildly heating the air-exposed sample (*e.g.*, between 70 and 100 °C; under $N_2$); the EPR intensity further increases after heating at 150 °C (under $N_2$; to give **M1**-150), and intensifies after heating at the higher temperature of 300 °C (to give **M1**-300). The IR spectra (Figure S18a) indicates the presence of alkyne units for samples **M1**-70, **M1**-100 and **M1**-150, whereas for **M1**-300, the alkyne peaks are absent, suggesting an extensively cyclized product.

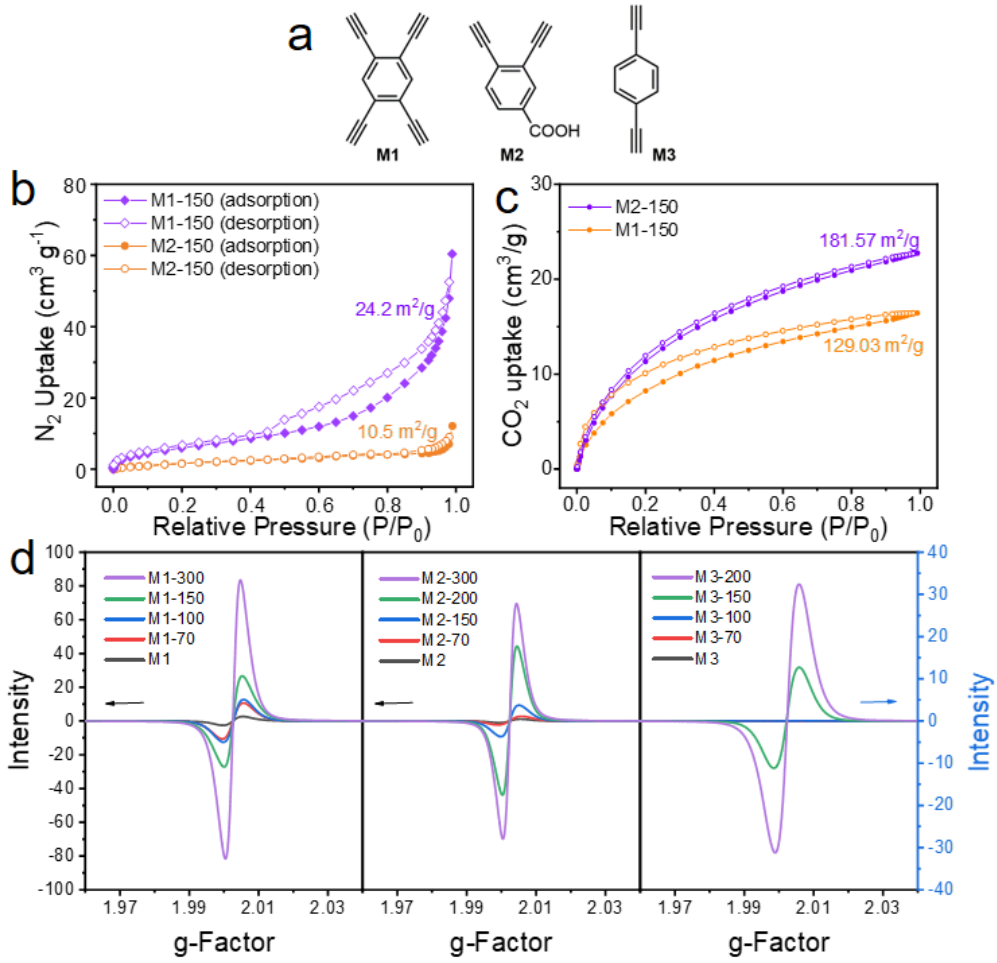


**Figure 4**. (a) The ethynylaryl molecules **M1**, **M2** and **M3**; (b) $N_2$ adsorption and desorption isotherms at 77 K for samples of **M1**-150 and **M2**-150; (c) $CO_2$ adsorption and desorption

isotherms at 273 K for samples of **M1**-150 and **M2**-150; (d) EPR spectra of **M1** and **M1**-T (T = 70, 100, 150, 300); **M2** and **M2**-T (T = 70, 150, 200, 300); **M3** and **M3**-T (T = 70, 100, 150, 200) at 298 K.

Compared with **M1**, **M2** contains only one pair of neighboring ethynyl groups, and shows distinct but weaker EPR signals after air-exposure and heating at lower temperatures (*e.g.*, 70 °C; Figure 4d). But the EPR signal (same amount 8.0 mg) becomes similarly strong after heating at higher temperatures (*e.g.*, 150 °C). Both the alkyne C–H and C–C IR stretches for **M2** disappeared after heating at 150 °C, indicating extensive cyclization at this temperature. Heating at 300 °C resulted in slightly strong EPR signal. Both **M1**-150 and **M2**-150 exhibit small $N_2$ uptake (77 K), but larger $CO_2$ uptake (273 K; BET surface areas 182 and 129 $m^2/g$, respectively); indicating microporosity for these heated samples (both are insoluble solids).

By contrast, **M3** contains no neighboring ethynyl groups, and its air-exposed and heated sample (*e.g.*, 100 °C) do not develop significant EPR signals. But at 150 °C, a significant EPR signal emerges, which further intensifies at the higher temperature of 200 °C. This comparison suggests neighboring alkynyl groups to be more effective for radical formation at lower temperature (Figure 4d). Out of precaution against explosion, fresh powder samples of **M1**–**M3** were never directly heated above 70 °C (they were first either exposed to air or heated at 70 °C for several hours).

The radicals present in these thermally annealed products are durable and concentrated. Most importantly, these radical-rich solids exhibit significantly broadened intense absorption covering the whole UV-visible spectral range even reaching NIR region when compared with their pristine analogues (*e.g.*, **M1** and **M2** showing significantly red-shifted absorption reaching NIR region (Figure S21), highlighting the extensive conjugated structures as well as the radical-rich nature of

the solid samples. In particular, Zr**L3** maintains the crystallinity even after thermal annealing at 400 ºC, thus allowing for easier monitoring of sample stability. Therefore, Zr**L3** and its thermally annealed forms were chosen here for photothermal conversion studies. Under one-sun irradiation (420–2500 nm) simulated with a xenon lamp at 0.1 W $cm^{-2}$, Zr**L3** and thermally annealed products (30 mg of samples) also exhibited photothermal conversion. Specifically, temperature change after eight-minute irradiation recorded for Zr**L3** is 18.3 ºC while those increase together with elevating annealing temperatures and reach highest for Zr**L3**-400 (ΔT: Zr**L3**-300 = 24.5 ºC; Zr**L3**-350 = 27.3 ºC; Zr**L3**-400 = 34.2 ºC) (Figure 5b). The best photothermal conversion efficiency of Zr**L3**-400 over pristine analogue and other counterparts thermally annealed at lower temperatures highlights broad absorption and abundant radicals as crucial components to execute effective photothermal conversion. All of them showed higher ΔT along with increasing powers of light source (0.1, 0.2, 0.3 and 0.5 W $cm^{-2}$) with Zr**L3**-400 reaching the maximum temperature of 112.6 ºC at the highest irradiation power (0.5 W $cm^{-2}$) (Figure S25). Noteworthily, all these radical-rich solids showed excellent anti-photobleaching property, as reflected by consistent ΔT throughout five cycles of xenon-lamp on-off irradiation (Figure 5c and Figures S22–24b). More importantly, all these solids are operationally stable during photothermal study, as revealed by the consistent PXRD patterns and FT-IR profiles of Z**rL3**-300, Zr**L3**-350 and Zr**L3**-400 before and after cycling photothermal experiments (Figure S26). Substantial improvement of photothermal conversion capacity by thermal annealing of crystalline solids offers opportunities towards photothermally active crystalline materials *via* easily accessible modification of frameworks.

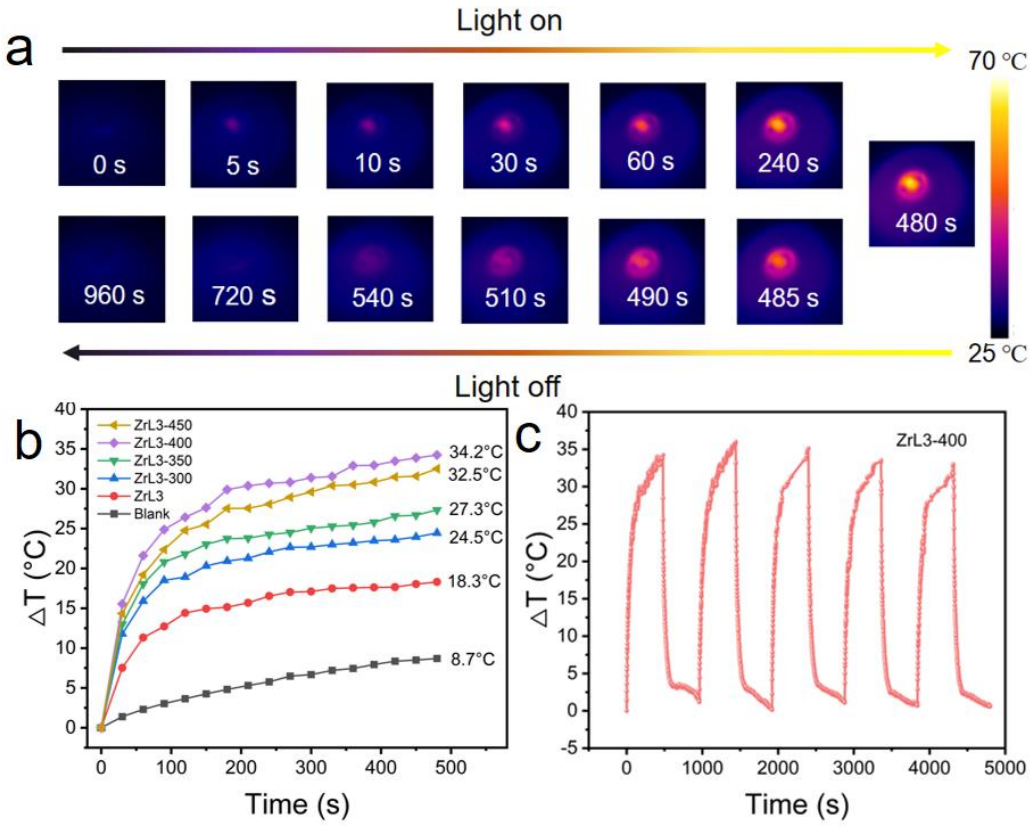


**Figure 5**. (a) The IR thermal images Zr**L3**-400 (30 mg) under a xenon lamp (0.1 W $cm^{-2}$, one-sun) and then with the xenon lamp turned off; (b) Photothermally induced temperature change of Zr**L3** and Zr**L3**-T (T = 300, 350, 400, 450) under xenon lamp irradiation (0.1 W $cm^{-2}$, one-sun); (c) Anti-photobleaching property of Zr**L3**-400 (30 mg) during five cycles of the heating−cooling process.

## 4. CONCLUSIONS

In conclusion, stable and concentrated organic radicals can be readily generated by heating alkynylaromatic molecules. The thermocyclization reactions thus triggered are extensive and vigorous: as no catalysts were added for channeling the reaction pathways, the annulated products are defect-rich and mixed, with the associated radical species stabilized by the resulted large (*e.g.*, nanographene-like) π-systems. Further characterization of the annulated products would be

informative. In spite of not being ordered, the resultant radical-rich carbonaceous solid can open new grounds for applications, especially because of their stable porosity and polarizable π-system (*e.g.*, being black, highly absorbing solids). After all, activated carbon and ion-exchange resin, as two major industrial porous materials, are both non-ordered structures.

We close with some flashback. This simple and surprising discovery traces back to our fundamental curiosity about backfolded molecules as building blocks for exploring framework materials. The backfolded linker design was executed in the form of the *o*-alkynyl motifs, while our long-standing focus on the sulfur (thioether and mercaptan) functions has led us to build many of these onto the backfolded linker scaffold (as in **L3** here). Sulfur groups are known for their propensity to form and stabilize radical species, so we tested the presence of radicals in the thermally treated framework solid Zr**L3**. The strong and stable radicals led us to suspect the generality of this observation, and--wenn schon, denn schon—to test for radicals in the simplest, all-too-familiar diethynyl benzenes.

## ASSOCIATED CONTENT

The Supporting Information is available free of charge at https://pubs.acs.org/doi/XXX/acs.inorgchem.XXX. TGA plot, IR and EPR spectra, solution $^{1}H/^{13}C$ NMR spectra, PXRD.

## AUTHOR INFORMATION

Corresponding Author

Jun He − School of Chemical Engineering and Light Industry, Guangdong University of Technology, Guangzhou 510006, China; orcid.org/0000-0001-7062-4001; Email: junhe@gdut.edu.cn.

Zhengtao Xu − Institute of Materials Research and Engineering (IMRE), Agency for Science, Technology and Research (A*STAR), 2 Fusionopolis Way, Singapore, 138634, Republic of Singapore; orcid.org/0000-0002-7408-4951; E-mail: Zhengtao@imre.a-star.edu.sg.

Authors

Dong-Ling Kuang − School of Chemical Engineering and Light Industry, Guangdong University of Technology, Guangzhou 510006, Guangdong, China.

Jian-Rong Li − School of Chemical Engineering and Light Industry, Guangdong University of Technology, Guangzhou 510006, Guangdong, China.

Jieying Hu − School of Chemical Engineering and Light Industry, Guangdong University of Technology, Guangzhou 510006, Guangdong, China.

Lai-Hon Chung − School of Chemical Engineering and Light Industry, Guangdong University of Technology, Guangzhou 510006, China; orcid.org/0000-0002-0482-1362

Parijat Borah − Institute of Materials Research and Engineering (IMRE), Agency for Science, Technology and Research (A*STAR), 2 Fusionopolis Way, Singapore, 138634, Republic of Singapore.

Complete contact information is available at:

https://pubs.acs.org/XXX/acs.inorgchem.XXX.

## Notes

The authors declare no competing financial interest.

## ACKNOWLEDGMENT

J. H. and L.-H. C. acknowledge the fundings by the National Natural Science Foundation of China (22371054, 22301045), the Foundation of Basic and Applied Basic Research of Guangdong Province (2020B1515120024), Science and Technology Planning Project of Guangdong Province (2021A0505030066), Science and Technology Program of Guangzhou (202201010244). Z. X. acknowledges a startup fund from A*STAR (SC25/22-119116).

## REFERENCES

1. Chen, Z. X.; Li, Y.; Huang, F., Persistent and Stable Organic Radicals: Design, Synthesis, and Applications. *Chem* **2021**, *7*, 288-332.

2. Hicks, R. G., What's new in stable radical chemistry? *Org. Biomol. Chem.* **2007**, *5*, 1321-38.

3. Chen, F.; Guan, X.; Li, H.; Ding, J.; Zhu, L.; Tang, B.; Valtchev, V.; Yan, Y.; Qiu, S.; Fang, Q., Three-Dimensional Radical Covalent Organic Frameworks as Highly Efficient and Stable Catalysts for Selective Oxidation of Alcohols. *Angew. Chem. Int. Ed.* **2021**, *60*, 22230-22235.

4. Lau, M.-T.; Li, Z.; Wong, W.-Y., Metallopolymers with Ferrocenyl and TEMPO Radical Units and Thermoelectric Properties of their Composites with Single-Wall Carbon Nanotubes. *Macromol. Chem. Phys.* **2023**, *224*, 2200419.

5. Chen, S.; Ju, Y.; Zhang, H.; Zou, Y.; Lin, S.; Li, Y.; Wang, S.; Ma, E.; Deng, W.; Xiang, S.; Chen, B.; Zhang, Z., Photo Responsive Electron and Proton Conductivity within a Hydrogen-Bonded Organic Framework. *Angew Chem Int Ed* **2023**, *62*, e202308418.

6. Dong, C.; Chu, J.; Cao, L.; Cui, F.; Liang, S.; Zhang, X.; Tao, X.; Wang, H.-G.; Zhu, G., A Three-Dimensional Silicon-Diacetylene Porous Organic Radical Polymer. *CCS Chem* **2023**, *5*, 607-615.

7. Wang, K.; Kang, X.; Yuan, C.; Han, X.; Liu, Y.; Cui, Y., Porous 2D and 3D Covalent Organic Frameworks with Dimensionality-Dependent Photocatalytic Activity in Promoting Radical Ring-Opening Polymerization. *Angew. Chem. Int. Ed.* **2021**, *60*, 19466-19476.

8. Nguyen, T. P.; Easley, A. D.; Kang, N.; Khan, S.; Lim, S. M.; Rezenom, Y. H.; Wang, S.; Tran, D. K.; Fan, J.; Letteri, R. A.; He, X.; Su, L.; Yu, C. H.; Lutkenhaus, J. L.; Wooley, K. L., Polypeptide organic radical batteries. *Nature* **2021**, *593*, 61-66.

9. Xie, Y.; Zhang, K.; Yamauchi, Y.; Oyaizu, K.; Jia, Z., Nitroxide radical polymers for emerging plastic energy storage and organic electronics: fundamentals, materials, and applications. *Mater. Horiz.* **2021**, *8*, 803-829.

10. Kawata, S.; Pu, Y. J.; Saito, A.; Kurashige, Y.; Beppu, T.; Katagiri, H.; Hada, M.; Kido, J., Singlet Fission of Non-polycyclic Aromatic Molecules in Organic Photovoltaics. *Adv. Mater.* **2016**, *28*, 1585-90.

11. Zeng, M.; Wang, X.; Ma, R.; Zhu, W.; Li, Y.; Chen, Z.; Zhou, J.; Li, W.; Liu, T.; He, Z.; Yan, H.; Huang, F.; Cao, Y., Dopamine Semiquinone Radical Doped PEDOT:PSS: Enhanced Conductivity, Work Function and Performance in Organic Solar Cells. *Adv. Energy Mater.* **2020,** *10*, 2000743.

12. Phan, H.; Herng, T. S.; Wang, D.; Li, X.; Zeng, W.; Ding, J.; Loh, K. P.; Shen Wee, A. T.; Wu, J., Room-Temperature Magnets Based on 1,3,5-Triazine-Linked Porous Organic Radical Frameworks. *Chem* **2019**, *5*, 1223-1234.

13. London, A. E.; Chen, H.; Sabuj, M. A.; Tropp, J.; Saghayezhian, M.; Eedugurala, N.; Zhang, B. A.; Liu, Y.; Gu, X.; Wong, B. M.; Rai, N.; Bowman, M. K.; Azoulay, J. D., A high-spin ground-state donor-acceptor conjugated polymer. *Sci. Adv.* **2019**, *5*, eaav2336.

14. Thorarinsdottir, A. E.; Harris, T. D., Metal-Organic Framework Magnets. *Chem. Rev.* **2020**, *120*, 8716-8789.

15. Minguez Espallargas, G.; Coronado, E., Magnetic functionalities in MOFs: from the framework to the pore. *Chem. Soc. Rev.* **2018**, *47*, 533-557.

16. Lu, B.; Chen, Y.; Li, P.; Wang, B.; Mullen, K.; Yin, M., Stable radical anions generated from a porous perylenediimide metal-organic framework for boosting near-infrared photothermal conversion. *Nat. Commun.* **2019**, *10*, 767.

17. Chan, J. M. W.; Wojtecki, R. J.; Sardon, H.; Lee, A. L. Z.; Smith, C. E.; Shkumatov, A.; Gao, S.; Kong, H.; Yang, Y. Y.; Hedrick, J. L., Self-Assembled, Biodegradable Magnetic Resonance Imaging Agents: Organic Radical-Functionalized Diblock Copolymers. *ACS Macro Lett.* **2017**, *6*, 176-180.

18. Lin, H.; Yang, Y.; Hsu, Y.-C.; Zhang, J.; Welton, C.; Afolabi, I.; Loo, M.; Zhou, H.-C., Metal–Organic Frameworks for Water Harvesting and Concurrent Carbon Capture: A Review for Hygroscopic Materials. *Adv. Mater.* **2023**, 2209073.

19. Zhang, P.; Luo, Q.-C.; Zhu, Z.; He, W.; Song, N.; Lv, J.; Wang, X.; Zhai, Q.-G.; Zheng, Y.-Z.; Tang, J., Radical-Bridged Heterometallic Single-Molecule Magnets Incorporating Four Lanthanoceniums. *Angew. Chem. Int. Ed.* **2023**, *62*, e202218540.

20. Jiao, L.; Jiang, H.-L., Metal-organic frameworks for catalysis: Fundamentals and future prospects. *Chin. J. Catal.* **2023,** *45*, 1-5.

21. Zhang, Y.-N.; Li, Q.-F.; Chen, B.-B.; Lan, Y.-Z.; Cheng, J.-W.; Yang, G.-Y., $Na_3B_6O_{10}(HCOO)$: an ultraviolet nonlinear optical sodium borate-formate. *Inorg. Chem. Front.* **2022**, *9*, 5032-5038.

22. Xu, C.; Pan, Y.; Wan, G.; Liu, H.; Wang, L.; Zhou, H.; Yu, S.-H.; Jiang, H.-L., Turning on Visible-Light Photocatalytic C−H Oxidation over Metal–Organic Frameworks by Introducing Metal-to-Cluster Charge Transfer. *J. Am. Chem. Soc.* **2019**, *141* (48), 19110-19117.

23. Xie, L. S.; Skorupskii, G.; Dinca, M., Electrically Conductive Metal-Organic Frameworks. *Chem. Rev.* **2020,** *120*, 8536-8580.

24. Faust, T. B.; D'Alessandro, D. M., Radicals in metal–organic frameworks. *RSC Adv.* **2014**, *4*, 17498-17512.

25. Kim, Y.; Byeon, J. E.; Jeong, G. Y.; Kim, S. S.; Song, H.; Lee, E., Highly Stable 1,2-Dicarbonyl Radical Cations Derived from N-Heterocyclic Carbenes. *J. Am. Chem. Soc.* **2021**, *143*, 8527-8532.

26. Ji, L.; Shi, J.; Wei, J.; Yu, T.; Huang, W., Air-Stable Organic Radicals: New-Generation Materials for Flexible Electronics? *Adv. Mater.* **2020**, *32*, e1908015.

27. Zeng, W.; Wu, J., Open-Shell Graphene Fragments. *Chem* **2021**, *7*, 358-386.

28. Xiang, Q.; Guo, J.; Xu, J.; Ding, S.; Li, Z.; Li, G.; Phan, H.; Gu, Y.; Dang, Y.; Xu, Z.; Gong, Z.; Hu, W.; Zeng, Z.; Wu, J.; Sun, Z., Stable Olympicenyl Radicals and Their pi-Dimers. *J. Am.. Chem Soc* **2020**, *142*, 11022-11031.

29. Li, G.; Han, Y.; Zou, Y.; Lee, J. J. C.; Ni, Y.; Wu, J., Dearomatization Approach Toward a Superbenzoquinone-Based Diradicaloid, Tetraradicaloid, and Hexaradicaloid. *Angew. Chem. Int. Ed.* **2019**, *58*, 14319-14326.

30. Rana, A.; Hong, Y.; Gopalakrishna, T. Y.; Phan, H.; Herng, T. S.; Yadav, P.; Ding, J.; Kim, D.; Wu, J., Stable Expanded Porphycene-Based Diradicaloid and Tetraradicaloid. *Angew. Chem. Int. Ed.* **2018**, *57*, 12534-12537.

31. Li, Y.; Jia, Z.; Xiao, S.; Liu, H.; Li, Y., A method for controlling the synthesis of stable twisted two-dimensional conjugated molecules. *Nat. Commun.* **2016**, *7*, 11637.

32. Shimizu, D.; Osuka, A., Porphyrinoids as a platform of stable radicals. *Chem. Sci.* **2018**, *9*, 1408-1423.

33. Ye, X.; Chung, L. H.; Li, K.; Zheng, S.; Wong, Y. L.; Feng, Z.; He, Y.; Chu, D.; Xu, Z.; Yu, L.; He, J., Organic radicals stabilization above 300 $^{o}$C in Eu-based coordination polymers for solar steam generation. *Nat. Commun.* **2022**, *13*, 6116.

34. Zhong, Y.-H.; Chung, L.-H.; Zhao, S.-Y.; Feng, Z.; Hu, J.; Li, N.; Liao, W.-M.; Wong, W.-Y.; Yu, L.; He, J., Design and facile synthesis of a photothermally active metal–organic framework bearing persistent radicals via post-synthetic thermal annealing. *J. Mater. Chem. A* **2022**, *10*, 23195-23203.

35. Desmet, C. M.; Tran, L. B. A.; Danhier, P.; Gallez, B., Characterization of a clinically used charcoal suspension for in vivo EPR oximetry. *Magn. Reson. Mater. Phys. Biol. Med.* **2019**, *32*, 205-212.

36. Lan, M.; Beghein, N.; Charlier, N.; Gallez, B., Carbon blacks as EPR sensors for localized measurements of tissue oxygenation. *Magn. Reson. Med.* **2004**, *51*, 1272-8.

37. Hu, J.; Deng, X.; Zhang, H.; Diao, Y.; Cheng, S.; Zheng, S. L.; Liao, W. M.; He, J.; Xu, Z., Linker Deficiency, Aromatic Ring Fusion, and Electrocatalysis in a Porous Ni8-Pyrazolate Network. *Inorg. Chem.* **2021**, *60*, 161-166.

38. Cheng, S.; Xin, Y.; Hu, J.; Feng, W.; Ahn, D.; Zeller, M.; He, J.; Xu, Z., Invisible Silver Guests Boost Order in a Framework That Cyclizes and Deposits $Ag_3Sb$ Nanodots. *Inorg. Chem.* **2021**, *60*, 5757-5763.

39. Cheng, S.; Ma, T.; Xu, X.; Du, P.; Hu, J.; Xin, Y.; Ahn, D.; He, J.; Xu, Z., A Ferrocene Metal-Organic Framework Solid for Fe-Loaded Carbon Matrices and Nanotubes: High-Yield Synthesis and Oxygen Reduction Electrocatalysis. *Inorg. Chem.* **2021**, *60*, 17315-17324.

40. Diao, Y.; Hu, J.; Cheng, S.; Ma, F.; Li, M. Q.; Hu, X.; Li, Y. Y.; He, J.; Xu, Z., Dense Alkyne Arrays of a Zr(IV) Metal-Organic Framework Absorb $Co_2(CO)_8$ for Functionalization. *Inorg. Chem.* **2020**, *59*, 5626-5631.

41. Cheng, S.; Tieu, P.; Gao, W.; Hu, J.; Feng, W.; He, J.; Pan, X.; Xu, Z., Crystallinity after decarboxylation of a metal-carboxylate framework: indestructible porosity for catalysis. *Dalton Trans.* **2020**, *49*, 11902-11910.

42. Hou, Y. L.; Li, M. Q.; Cheng, S.; Diao, Y.; Vilela, F.; He, Y.; He, J.; Xu, Z., Dramatic improvement of stability by in situ linker cyclization of a metal-organic framework. *Chem. Commun.* **2018**, *54*, 9470-9473.

43. Wu, J.; Pisula, W.; Müllen, K., Graphenes as Potential Material for Electronics. *Chem. Rev.* **2007**, *107*, 718-747.

44. Tsefrikas, V. M.; Scott, L. T., Geodesic Polyarenes by Flash Vacuum Pyrolysis. *Chem. Rev.* **2006**, *106*, 4868-4884.

45. Xiao, X.; Hoye, T. R., The domino hexadehydro-Diels-Alder reaction transforms polyynes to benzynes to naphthynes to anthracynes to tetracynes and beyond?. *Nat. Chem.* **2018**, *10*, 838-844.

46. Miyawaki, K.; Kawano, T.; Ueda, I., Synthesis and Properties of Functionalized [6] Helicenes by the Thermal Domino Radical Cycloaromatization of Acyclic Polyynes. *Polycycl. Aromat. Comp.* **2001**, *19*, 133-154.

47. Chen, C.-C.; Chin, L.-Y.; Yang, S.-C.; Wu, M.-J., Synthetic Development and Mechanistic Study on Pd(II)-Catalyzed Cyclization of Enediynes to Benzo[a]carbazoles. *Org. Lett.* **2010**, *12*, 5652-5655.

48. Ding, N.; Li, H. W.; Feng, X.; Wang, Q. Y.; Wang, S.; Ma, L.; Zhou, J. W.; Wang, B., Partitioning MOF-5 into Confined and Hydrophobic Compartments for Carbon Capture under Humid Conditions. *J. Am. Chem. Soc.* **2016**, *138*, 10100-10103.

49. Chmiola, J.; Yushin, G.; Gogotsi, Y.; Portet, C.; Simon, P.; Taberna, P. L., Anomalous Increase in Carbon Capacitance at Pore Sizes Less Than 1 Nanometer. *Science* **2006**, *313*, 1760-1763.

50. Zhu, Y. H.; Shao, P. P.; Hu, L. Y.; Sun, C.; Li, J.; Feng, X.; Wang, B., Construction of Interlayer Conjugated Links in 2D Covalent Organic Frameworks via Topological Polymerization. *J. Am. Chem. Soc*. **2021**, *143*, 7897-7902.

51. Guo, Y.; Chang, R.; Fu, Z.; Zhou, C.-Y.; Guo, Z., Heterogeneous visible-light promoted dehydrogenative [4 + 2] annulation of benzothioamides and alkynes under aerobic conditions. *Green. Chem.* **2023**, *25*, 5206-5212.

52. Huang, L.; Eedugurala, N.; Benasco, A.; Zhang, S.; Mayer, K. S.; Adams, D. J.; Fowler, B.; Lockart, M. M.; Saghayezhian, M.; Tahir, H.; King, E. R.; Morgan, S.; Bowman, M. K.; Gu, X.; Azoulay, J. D., Open‐Shell Donor–Acceptor Conjugated Polymers with High Electrical Conductivity. *Adv. Funct. Mater.* **2020**, *30* , 1909805.

53. Yang, K.; Zhang, X.; Harbuzaru, A.; Wang, L.; Wang, Y.; Koh, C.; Guo, H.; Shi, Y.; Chen, J.; Sun, H.; Feng, K.; Ruiz Delgado, M. C.; Woo, H. Y.; Ortiz, R. P.; Guo, X., Stable Organic Diradicals Based on Fused Quinoidal Oligothiophene Imides with High Electrical Conductivity. *J. Am. Chem. Soc.* **2020**, *142*, 4329-4340.

54. Yuan, D.; Guo, Y.; Zeng, Y.; Fan, Q.; Wang, J.; Yi, Y.; Zhu, X., Air-Stable n-Type Thermoelectric Materials Enabled by Organic Diradicaloids. *Angew. Chem. Int. Ed.* **2019**, *58*, 4958-4962.